

A Unique Chromosomal Rearrangement in the *Cryptococcus neoformans* var. *grubii* Type Strain Enhances Key Phenotypes Associated with Virulence

Author

Morrow, Carl A, Lee, I Russel, Chow, Eve WL, Ormerod, Kate L, Goldinger, Anita, Byrnes, Edmond J, Nielsen, Kirsten, Heitman, Joseph, Schirra, Horst Joachim, Fraser, James A

Published

2012

Journal Title

mBio

Version

Version of Record (VoR)

DOI

[10.1128/mBio.00310-11](https://doi.org/10.1128/mBio.00310-11)

Rights statement

© 2012 Morrow et al. This is an open-access article distributed under the terms of the Creative Commons Attribution-Noncommercial-Share Alike 3.0 Unported License, which permits unrestricted noncommercial use, distribution, and reproduction in any medium, provided the original author and source are credited.

Downloaded from

<http://hdl.handle.net/10072/413123>

Griffith Research Online

<https://research-repository.griffith.edu.au>

A Unique Chromosomal Rearrangement in the *Cryptococcus neoformans* var. *grubii* Type Strain Enhances Key Phenotypes Associated with Virulence

Carl A. Morrow,^{a,b} I. Russel Lee,^{a,b} Eve W. L. Chow,^{a,b} Kate L. Ormerod,^{a,b} Anita Goldinger,^b Edmond J. Byrnes III,^c Kirsten Nielsen,^d Joseph Heitman,^e Horst Joachim Schirra,^{b,f} and James A. Fraser^{a,b}

Australian Infectious Diseases Research Centre, University of Queensland, Brisbane, Australia^a; School of Chemistry and Molecular Biosciences, University of Queensland, Brisbane, Australia^b; Department of Medicine, Johns Hopkins University School of Medicine, Baltimore, Maryland, USA^c; Department of Microbiology, Medical School, University of Minnesota, Minneapolis, Minnesota, USA^d; Department of Molecular Genetics and Microbiology, Duke University Medical Center, Durham, North Carolina, USA^e; and Centre for Advanced Imaging, University of Queensland, Brisbane, Australia^f

ABSTRACT The accumulation of genomic structural variation between closely related populations over time can lead to reproductive isolation and speciation. The fungal pathogen *Cryptococcus* is thought to have recently diversified, forming a species complex containing members with distinct morphologies, distributions, and pathologies of infection. We have investigated structural changes in genomic architecture such as inversions and translocations that distinguish the most pathogenic variety, *Cryptococcus neoformans* var. *grubii*, from the less clinically prevalent *Cryptococcus neoformans* var. *neoformans* and *Cryptococcus gattii*. Synteny analysis between the genomes of the three *Cryptococcus* species/varieties (strains H99, JEC21, and R265) reveals that *C. neoformans* var. *grubii* possesses surprisingly few unique genomic rearrangements. All but one are relatively small and are shared by all molecular subtypes of *C. neoformans* var. *grubii*. In contrast, the large translocation peculiar to the *C. neoformans* var. *grubii* type strain is found in all tested subcultures from multiple laboratories, suggesting that it has possessed this rearrangement since its isolation from a human clinical sample. Furthermore, we find that the translocation directly disrupts two genes. The first of these encodes a novel protein involved in metabolism of glucose at human body temperature and affects intracellular levels of trehalose. The second encodes a homeodomain-containing transcription factor that modulates melanin production. Both mutations would be predicted to increase pathogenicity; however, when recreated in an alternate genetic background, these mutations do not affect virulence in animal models. The type strain of *C. neoformans* var. *grubii* in which the majority of molecular studies have been performed is therefore atypical for carbon metabolism and key virulence attributes.

IMPORTANCE The fungal pathogen *Cryptococcus* is a major cause of mortality among the immunocompromised population, primarily in AIDS patients of sub-Saharan Africa. Most research into the particular variety of *Cryptococcus* responsible for the vast majority of infections, *Cryptococcus neoformans* var. *grubii*, is performed using the type strain isolated in 1978 from a Hodgkin's disease patient from North Carolina. We have determined that this particular isolate contains a chromosomal translocation that directly interrupts two genes, which all descendants of this strain from various research laboratories appear to possess. Disruption of these two genes affects multiple virulence factors of *Cryptococcus*, particularly the ability to grow at human body temperature, which could have wide-ranging implications for molecular genetic studies and virulence assays using this important strain.

Received 29 December 2011 Accepted 5 January 2012 Published 28 February 2012

Citation Morrow CA, et al. 2012. A unique chromosomal rearrangement in the *Cryptococcus neoformans* var. *grubii* type strain enhances key phenotypes associated with virulence. *mBio* 3(2):e00310-11. doi:10.1128/mBio.00310-11.

Editor Judith Berman, University of Minnesota

Copyright © 2012 Morrow et al. This is an open-access article distributed under the terms of the Creative Commons Attribution-Noncommercial-Share Alike 3.0 Unported License, which permits unrestricted noncommercial use, distribution, and reproduction in any medium, provided the original author and source are credited.

Address correspondence to James A. Fraser, jafrazer@uq.edu.au.

Increasing numbers of completed genome sequences have made apparent that large changes in genome structure play a much greater role in the generation of phenotypic diversity between species than previously appreciated. While small mutations such as single nucleotide polymorphisms have long been associated with disease states and phenotypic variation in humans, larger structural alterations have recently been revealed to be at least as important in generating variation (1). Furthermore, recent theories propose that the suppression of recombination associated with large chromosomal rearrangement events allows for accumula-

tion of mutations, reproductive isolation without gene flow in freely mixing populations, local adaptation, and specialization (2). Direct association of chromosomal rearrangements with local adaptation and speciation has since been demonstrated for fungi (3), plants (4), and insects (5). Both the ubiquity of structural variants within individual human genomes and contributions to various disease states have also been demonstrated (6).

Structural variants or gross chromosomal rearrangements can have profound influences on phenotype and encompass large changes such as intra- and interchromosomal translocations,

large duplications and deletions, copy number variations, inversions, and whole-chromosome aneuploidies. Seminal studies from *Drosophila* species have shown that inversions can delineate closely related species (7), while inversions characterize the sex-determining chromosomes in a variety of species, including humans (8, 9). Translocations can suppress recombination and sequester sets of genes in a manner similar to that of inversions and can alter gene expression around breakpoints and along their length through tertiary chromosome positioning (10). Large duplications of genes allow for specialization and sub- and neofunctionalization of duplicate copies, with the most famous being the whole-genome duplications of the Saccharomycetaceae yeasts and the teleost fishes (11, 12).

The opportunistic fungal pathogen *Cryptococcus neoformans* is a major cause of mortality in the immunocompromised population, causing an estimated 625,000 deaths per annum, primarily in areas where AIDS is endemic (13). The species consists of two varieties that diverged approximately 24.5 million years ago: *Cryptococcus neoformans* var. *grubii*, which causes the vast majority of infections, and *Cryptococcus neoformans* var. *neoformans*, which is far less clinically prevalent. The pathogenic *Cryptococcus* species complex is further demarcated into molecular subtypes: *C. neoformans* var. *grubii* comprises subtypes VNI, VNII, and VNB while *C. neoformans* var. *neoformans* is subtype VNIV. The sister species *Cryptococcus gattii*, which diverged 45 million years ago, comprises the subtypes VGI, VGII, VGIII, and VGIV and is generally considered a primary pathogen of healthy individuals, although both species have the capacity to infect immunocompetent and immunodeficient patients (14). The three groupings (*C. neoformans* var. *grubii*, *C. neoformans* var. *neoformans*, and *C. gattii*) display marked differences in distribution, ecology, morphology, epidemiology, and virulence.

Whether the two *C. neoformans* varieties represent separate species is currently under debate, as are proposals to raise the *C. gattii* molecular subtypes to the variety or perhaps species level (15, 16). Recent comparisons of completed *Cryptococcus* genome sequences have highlighted rearrangements between *C. neoformans* var. *neoformans* and *C. neoformans* var. *grubii* (17, 18), between *C. gattii* VGI and *C. gattii* VGII, and between *C. gattii* VGI/II and *C. neoformans* var. *neoformans* (16). As *C. neoformans* var. *grubii* is far more prevalent than the other two organisms in cryptococcal infections ($\geq 90\%$) and causes the majority of deaths worldwide, we were interested in structural variants at the chromosomal level that were unique to *C. neoformans* var. *grubii*. Changes in karyotype arise frequently in *Cryptococcus* during infection, suggesting that it may be a common mechanism to generate variation and adapt to the host environment (19, 20). Similar genomic microevolution has been linked with success of infection in fungal pathogens such as *Candida albicans* (21, 22). Interrogating such changes may elucidate modes of speciation in the pathogenic *Cryptococcus* species complex or suggest genetic mechanisms for the prevalence and virulence of *C. neoformans* var. *grubii*.

In this study, we compared the sequenced genome of the *C. neoformans* var. *grubii* type strain, H99, with those of the *C. neoformans* var. *neoformans* strain JEC21 and the *C. gattii* strain R265 using synteny analysis to identify translocations, duplications, deletions, and inversions. We found that *C. neoformans* var. *grubii* possesses very few unique genomic rearrangements; however, the single large translocation identified appears restricted to the type

strain of *C. neoformans* var. *grubii* and is shared by all subcultures tested. We find that it directly interrupts two genes, one encoding a protein involved in glucose metabolism during high-temperature growth and the other encoding a homeodomain-containing transcription factor that represses melanization. Despite the fact that these two genes impact multiple virulence factors, pathogenicity is unaffected in animal models. As H99 is the most intensively studied strain of *Cryptococcus* worldwide, this could have significant impacts on genetic and virulence studies in this important human pathogen.

RESULTS

Synteny analysis reveals surprisingly few genome rearrangements unique to *C. neoformans* var. *grubii*. To develop an understanding of the evolutionary significance and clinical consequences of large-scale genomic rearrangements in *C. neoformans* var. *grubii*, we performed pairwise comparisons using dot plot analysis on three of the available *Cryptococcus* pathogenic species complex genomes: *C. neoformans* var. *grubii* (strain H99), *C. neoformans* var. *neoformans* (strain JEC21), and *C. gattii* (strain R265). The widely distributed type strain H99 was isolated in 1978 from the cerebrospinal fluid of a 27-year-old Caucasian male being treated for Hodgkin's disease in North Carolina by John Perfect (23). Strain H99 is an important isolate as it is the foundation of molecular research in *Cryptococcus*. Pairwise analysis revealed broad synteny across the 14 chromosomes of the genomes, with the notable exceptions being the centromeres, the subtelomeric regions, and *MAT*. Large genomic rearrangements (greater than 1 kb) specific to *C. neoformans* var. *grubii* numbered eight in total. Six inversions were identified, two on chromosome 1 and one each on chromosomes 3, 7, 9, and 14; in addition, a small duplication is associated with the inversion on chromosome 14 and a large reciprocal translocation is present involving chromosomes 3 and 11 (Fig. 1). The ancestral state of chromosomes 3 and 11 is likely represented by the chromosomal arrangement in R265; JEC21 has undergone a pericentric inversion on chromosome 3, while H99 has undergone a translocation between chromosomes 3 and 11. Rearrangements peculiar to each genome were evident through our analyses, including previously identified events in *C. neoformans* var. *neoformans*: the introgression of *C. neoformans* var. *grubii*-specific sequence (the identity island) and a duplication and translocation involving JEC21 chromosomes 8 and 12 (17, 24).

These findings are consistent with those of Sun and Xu (18), who examined chromosomal rearrangements between *C. neoformans* var. *grubii* and *C. neoformans* var. *neoformans* and identified five translocations and 27 rearrangements. Our inclusion of *C. gattii* establishes that many of those changes are unique to *C. neoformans* var. *neoformans*. The five translocations comprise the telomere-telomere fusion and associated duplication identified by Fraser et al. (24), the pericentric inversion on JEC21 chromosome 3, and the chromosome 3/11 translocation in H99. There are seven *C. neoformans* var. *neoformans*-specific inversions, two on chromosome 1, two on chromosome 4, and one each on chromosomes 5, 7, and 14. Both *C. neoformans* var. *grubii* and *C. neoformans* var. *neoformans* possess separate inversions on chromosome 7 that share a common breakpoint. The remaining rearrangements identified in *C. neoformans* var. *neoformans* comprise the centromeres and *MAT*.

For the six *C. neoformans* var. *grubii*-unique inversions, five

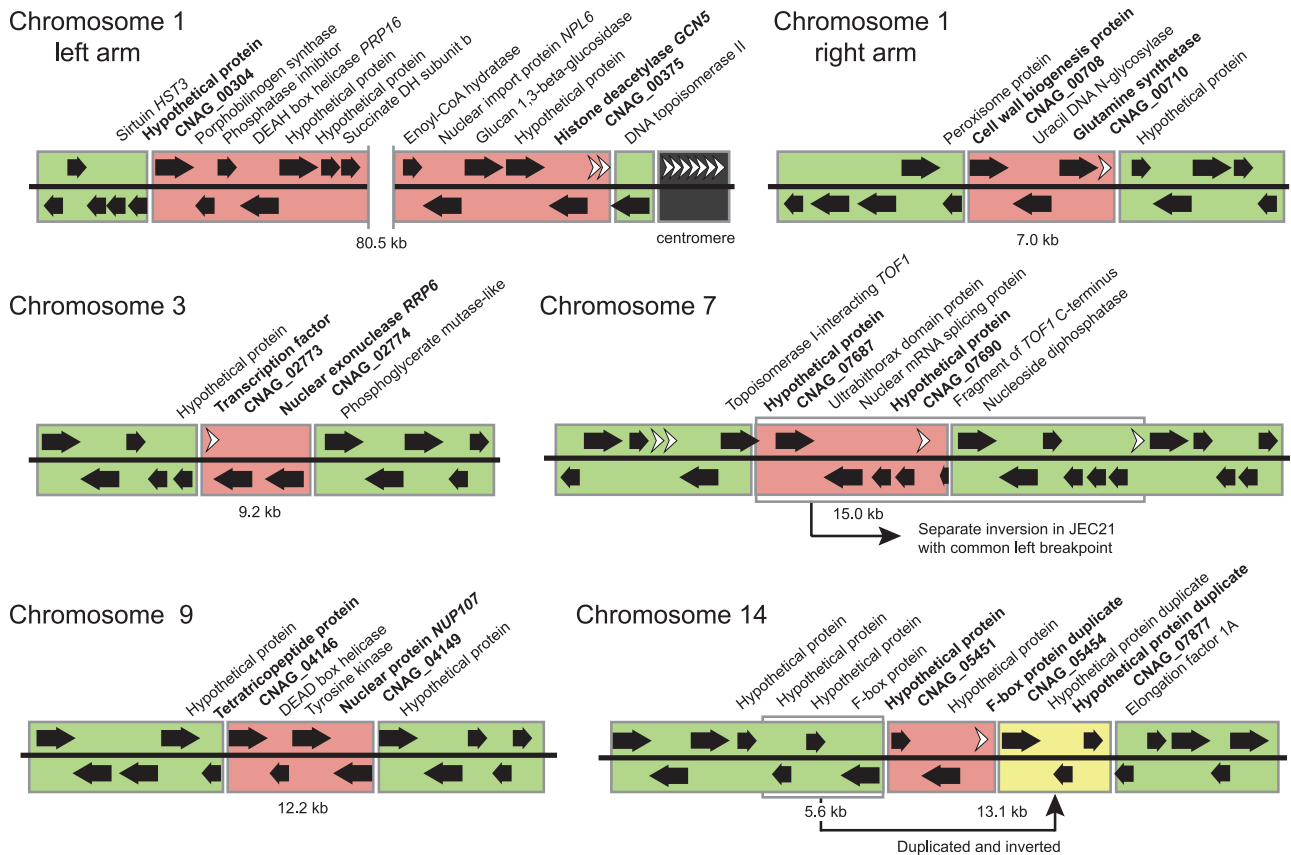


FIG 1 Inversions unique to the *C. neoformans* var. *grubii* genome. Green regions are syntenic with the *C. neoformans* var. *neoformans* and *C. gattii* genomes, while red regions are inverted and yellow indicates the duplication. Genes are represented by black arrows indicating direction of transcription, while white arrowheads represent transposable or repeated elements near inversion breakpoints. Images are not to scale. CoA, coenzyme A.

encompass only two to four genes, while one inversion on chromosome 1 captures 34 genes (Fig. 1). Most of the inversion breakpoints are intergenic, and all except the inversion on chromosome 9 are associated with a repeated or transposable element. One each of the breakpoints on chromosomes 1, 7, and 14 is within genes and creates novel 3' ends for the genes encoding DNA topoisomerase II Top2, the replication checkpoint component Top1, and elongation factor 1A Tif11. The inversion on H99 chromosome 14 also has an associated inverted duplication of 5,567 bp, which encompasses three genes.

The six inversions identified in H99 appear to be a synapomorphy of *C. neoformans* var. *grubii*. Genomic inversions can lead to altered expression of genes surrounding the breakpoints and contribute to speciation via suppression of homologous recombination. To investigate whether the six inversions identified in the *C. neoformans* var. *grubii* genome sequence are unique to strain H99 (a VNI isolate), we designed PCR assays to test for their presence or absence. All subcultures and progeny of H99 possessed the duplication and six inversions (see Fig. S1 in the supplemental material). The seven known amplified fragment length polymorphism (AFLP) subclades of molecular type VNI also possessed these seven rearrangements, as do molecular types VNII and VNB. Both *C. neoformans* var. *neoformans* VNIV and *C. gattii* VGII lack these features, confirming all seven traits to be characteristic of *C. neoformans* var. *grubii*.

Nucleotide *dS* rates are uniform across the chromosomal inversions. Chromosomal inversions lead to local suppression of recombination in affected chromosomal regions (25). For the *C. neoformans* var. *neoformans*/*C. neoformans* var. *grubii* split, we determined the *dS* (synonymous substitution) values for all genes contained within the *C. neoformans* var. *grubii*-specific inversions and compared them to those of flanking genes on both sides of the inversions. All six inversions had average *dS* values that were comparable to that of flanking regions (see Fig. S2 in the supplemental material). This suggests that the *C. neoformans* var. *grubii* common ancestor may have been geographically isolated and not have frequently undergone sexual reproduction with the *C. neoformans* var. *neoformans* ancestor, as there is no evidence of suppressed recombination across these regions. Furthermore, all inversion-associated genes had average *dN/dS* ratios (ratios of nonsynonymous to synonymous substitutions) of <1 , where values of >1 represent positive selection and values of <1 represent purifying selection (Fig. S2). Again, these ratios were similar to those of flanking genes.

The H99 translocation shows evidence of being produced via nonhomologous end joining and disrupts two genes. Of all the changes identified, only the translocation between chromosomes 3 and 11 appeared to be H99 specific. To investigate the origin of this genomic event, we interrogated an array of 80 diverse isolates via diagnostic PCR. The translocation was present exclusively in

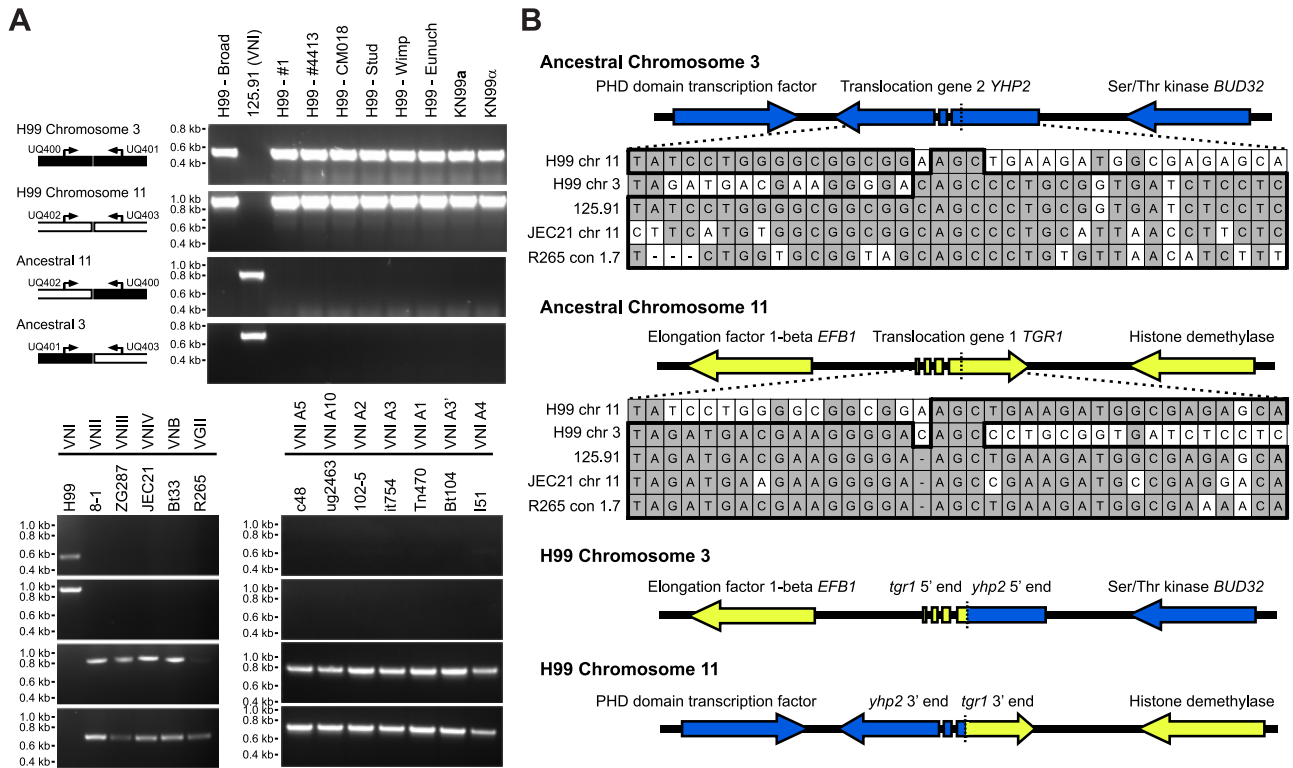


FIG 2 Identification and reconstruction of the H99 translocation. (A) Diagnostic PCR assay spanning the translocation boundary designed to produce an amplicon only when the translocation is present. Extended testing establishes that the translocation is present in all subcultures of H99 tested but absent from all other strains. (B) Alignment of the translocation breakpoints from H99, JEC21, R265, and VNI isolate 125.91. Note the presence of a microhomology, AGC, at the breakpoint, along with a single-base-pair insertion, A, before the microhomology on H99 chromosome 11. *In silico* reversal of the translocation and removal of the base pair insertion yields two complete ORFs without frameshift or nonsense mutations.

subcultures of strain H99 and its derivatives (Fig. 2 and results not shown), suggesting that it was present in the originally isolated H99 clinical sample. To more precisely characterize the chromosome 3/11 H99 translocation, the breakpoint regions were amplified and sequenced from the VNI isolate 125.91 (Fig. 2). There is a 3-bp microhomology at the breakpoint on both chromosomes, plus a single-base-pair insertion before the microhomology on chromosome 11, hallmarks of the translocation arising from non-homologous end joining (26). BLAST analysis of the breakpoint suggests that the translocation interrupts two genes such that the 5' ends of both genes converge on chromosome 3 while the 3' ends face away from each other on chromosome 11 (Fig. 2). If transcribed, the 5' fragments of both genes on the H99 chromosome would form relatively short truncated proteins appended with sequence from the antisense strands of the other gene. Careful re-annotation of these genes with reference to a number of fungal genomes suggests that both have been misannotated in the existing *Cryptococcus* genomes.

One gene disrupted in the H99 translocation, *TGR1*, is involved in metabolism of glucose at high temperature. Owing to the translocation, the shorter of the two translocation-associated genes is annotated as two separate open reading frames (ORFs) in the unpublished Broad Institute H99 assembly, with the 3' end on chromosome 11 (CNAG_01857) and the 5' end on chromosome 3 (CNAG_02713). The same gene is located on chromosome 3 in JEC21 (XM_569672), chromosome 3 in WM276 (CGB_C5260C), and supercontig 8 of R265 (CNBG_3377). The gene is 1,063 bp,

contains three introns, and yields a predicted protein of 300 amino acids. BLAST analysis reveals that the gene is widespread in the *Agaricomycotina*, appearing in 20 of 27 available genomes, but appears absent from all other fungal species. There are no characterized homologs and no predicted protein domains or secondary structure.

A deletion mutant constructed in VNB isolate Bt63 was tested with a wide variety of media, conditions, and stressors, including various carbon and nitrogen sources; extremes of pH and ionic and osmotic stress; oxidative, nitrosative, and sulfhydryl stress; low-iron and low-phosphate media; metal and metalloid stressors; extremes of temperature; UV resistance; cell wall- and cell membrane-perturbing agents; and CO₂ and O₂ stress. All tests were performed at both 30°C and 37°C to discriminate phenotypes that may be evident only during infection of a mammalian host. Over 70 conditions were tested in total. The majority of these tests were uninformative. However, although the mutant with the deletion of this first translocation gene in Bt63 had no phenotype at 30°C when cultured on minimal medium plus glucose, at 37°C the mutant showed increased growth compared to that of the wild type. We therefore dubbed the gene *TGR1*, for temperature-sensitive glucose-specific growth repressor 1 (Fig. 3). The phenotype was specific to the presence of glucose and was abolished when the mutant was grown on other sole carbon sources including mono-, di-, and trisaccharides; acetate; ethanol; glycerol; amino acids; and fatty acids (Fig. 3 and results not shown). The phenotype was also apparent when glucose was present and when

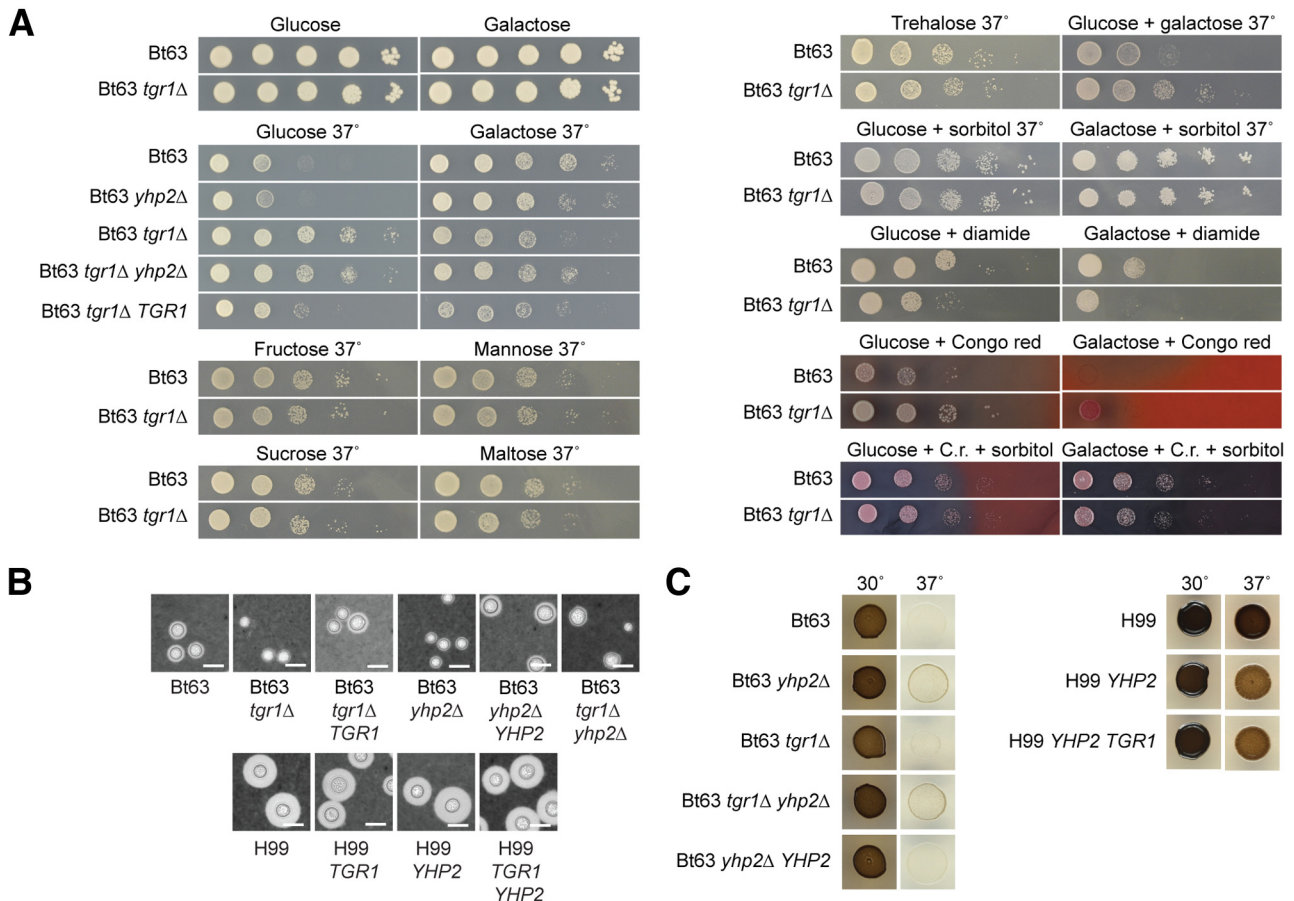


FIG 3 Reverse genetics in strain Bt63 and phenotypic characterization reveal roles for the two genes disrupted by the translocation observed in strain H99. (A) The two genes disrupted by the translocation, designated *YHP2* and *TGR1*, were deleted via homologous recombination in the VNB isolate Bt63. Tenfold serial dilutions of each strain were spotted onto YNB plates supplemented with the indicated carbon source, stressor, or osmotic stabilizer. The complemented strain Bt63 *tgr1*Δ *TGR1* displayed the wild-type Bt63 phenotype for all assays where it is not shown. (B) Polysaccharide capsule production visualized as a clear halo around the cell in an India ink stain. Bar = 10 μ m. (C) Melanization of strains on L-DOPA-containing medium. Melanized *Cryptococcus* cells turn brown-black.

other variables were altered, such as culture pH or nitrogen source (results not shown). Reperforming all other phenotypic tests with galactose substituted for glucose revealed no additional changes. In the presence of both glucose and any other carbon source tested, the glucose effect was dominant and growth was enhanced in the mutant at 37°C (Fig. 3). Reintroduction of *TGR1* into the Bt63 *tgr1*Δ strain yielded a wild-type phenotype under all conditions tested. To ensure that the truncated *tgr1*Δ-309 gene present in H99 was nonfunctional, we cloned the *tgr1*Δ-309/*yhp2*Δ-588 fusion construct from H99 and transformed it into the Bt63 *tgr1*Δ strain. The truncated version was unable to complement the phenotype of the Bt63 *tgr1*Δ strain on glucose at 37°C (results not shown).

As extremes of temperature can affect cell wall and cell membrane integrity, we tested the mutant on both glucose and galactose at 30°C and 37°C on compounds that perturb these structures. No common changes were observed on glucose and galactose when supplemented with caffeine, calcofluor white, or SDS; however, the *tgr1*Δ mutant grew better than did the wild type in the presence of Congo red irrespective of carbon source or temperature and displayed poorer growth on diamide (Fig. 3). Congo red is thought to interfere with β -1,3-glucan assembly in

the fungal cell wall by binding to the assembling β -1,3-glucan fibrils and preventing their close interactions, resulting in a loss of rigidity (27). Diamide oxidizes cellular thiol groups, especially protein cysteine sulfhydryl bonds, and induces pore formation in the cell wall (28). Consistent with these effects, supplementation of the medium with the osmotic stabilizer sorbitol, mannitol, or sucrose ablated high-temperature differences in growth between the wild type and mutant on glucose and galactose, as well as growth on Congo red, suggesting that the phenotype is related to cellular integrity (Fig. 3).

The second gene disrupted, *YHP2*, encodes a homeodomain-containing transcription factor. The second and larger of the two translocation-associated genes is located on chromosome 11 in JEC21 (XM_567674), chromosome 11 in WM276 (CGB_K2020C), and supercontig 7 of R265 (CNBG_3081). The gene is annotated as a single ORF at the Broad Institute (3' end only) on chromosome 11 (CNAG_01858). Reannotation revealed that the JEC21, WM276, and R265 annotations all excluded a section containing a putative homeodomain motif. The gene is 2,377 bp long, contains two introns, and yields a protein of 754 residues. Reciprocal best-hit BLAST analysis using the well-characterized fungal homeodomain proteins Cup9, Pho2, Tos8,

Yhp1, Yox1, MATalpha2, and HMRA1 from *Saccharomyces cerevisiae* did not reveal any clear orthologs to the predicted protein. Further BLAST analysis using just the 60-amino-acid homeodomain sequence revealed potential homologs in 25 of the 34 available basidiomycete genomes, although these display limited similarity outside the homeodomain itself. We named the second gene *YHP2*, for yeast homeodomain protein 2.

Testing a Bt63 *yhp2Δ* mutant on the same variety of nutrient sources, conditions, and stressors as those for the *tgr1Δ* strain yielded no phenotypes under any conditions (Fig. 3 and results not shown). No differences were observed between 30°C and 37°C. We also did not notice any epistatic effects on a *tgr1Δ yhp2Δ* double mutant, which was affected in the same fashion as was the *tgr1Δ* mutant on glucose at 37°C but did not show any novel phenotypes (Fig. 3).

Melanin production is repressed by the *YHP2* transcription factor. We next investigated effects of the single and double gene deletions on classical *Cryptococcus* virulence components: melanin, capsule, extracellular protease, urease, and phospholipase B. While no changes in production of extracellular proteins were observed for the *tgr1Δ*, *yhp2Δ*, and *tgr1Δ yhp2Δ* mutants (results not shown), all three exhibit a slightly reduced capsule size, which reverts to wild-type levels in the *tgr1Δ TGR1* and *yhp2Δ YHP2* complemented strains (Fig. 3). While the *tgr1Δ* mutant was indistinguishable from wild-type strains in the melanin assays, both the *yhp2Δ* and *tgr1Δ yhp2Δ* mutants showed a subtle but reproducible increase in melanin production at both 30°C and 37°C (Fig. 3). No changes in mating proficiency, filamentation, or antifungal resistance were observed (see Fig. S3 in the supplemental material; also results not shown).

Melanization and high-temperature growth on glucose are multigenic traits. Owing to the reciprocal translocation in chromosomes 3 and 11 of H99, at synapsis in meiosis I H99 chromosomes will form quadrivalents with the normal chromosomes 3 and 11 of Bt63. Only parental H99-type or Bt63-type chromosomes 3 and 11 should therefore be present together in any progeny, as mixed parent chromosome 3/11 segregants will be unbalanced and contain large deletions and duplications that should be fatal. To test this, we analyzed chromosomes of 16 meiotic progeny of H99 × Bt63 crosses using pulsed-field gel electrophoresis and probed Southern blots using probes to *TGR1* and *YHP2*. Eight of the progeny displayed bands consistent with a Bt63 karyotype, while the remaining eight displayed banding consistent with an H99 genotype (see Fig. S4 in the supplemental material). No hybrid combinations were observed, suggesting that the 50% of progeny bearing a nonparental set of chromosomes 3 and 11 are inviable. Consistent with this, basidiospore germination frequencies for two separate H99 × Bt63 crosses were below 50%, with the obtained values of 23.0% and 30.2% implying that further lethal phenotypes may have been segregating among the progeny. When tested for melanization, capsule production, and growth at 37°C in the presence of glucose, the phenotypes did not cosegregate with their parental karyotype in the 16 progeny, and we instead observed a gradient of phenotypes for all three conditions (Fig. S4). We hypothesize that these traits in *Cryptococcus* may be multigenic traits and that other contributing genes may obscure segregation of the deletion phenotypes.

Transcription of genes involved in melanin production is unaffected in the *yhp2Δ* mutant. Melanization in *Cryptococcus* is catalyzed by two laccases, Lac1 and Lac2, and is regulated by the

cyclic AMP (cAMP) pathway, although a variety of proteins and pathways are known to modulate activity (29). We therefore investigated potential targets of the Yhp2 transcription factor by examining changes in gene expression of components of the cAMP and mitogen-activated protein kinase (MAPK)-protein kinase C (PKC) pathway and the laccase genes *LAC1* and *LAC2*. No significant changes were observed in any of the genes tested (results not shown). This suggests that Yhp2 does not alter melanization through changes in expression of known signaling pathway components that control melanization, nor through changes in levels of *LAC1* or *LAC2* transcript.

Transcription of *HXX1* and components of stress response pathways are affected in the *tgr1Δ* mutant. Changes in growth on glucose, the most easily assimilable carbon source, have been observed previously in *Cryptococcus* mutants lacking peroxisome components (30) or trehalose biosynthesis (31, 32). These changes potentially involve cellular wall and membrane stresses and a dysregulation of glycolytic flux. Initially, we determined if *TGR1* gene expression was regulated in response to increased temperature using quantitative reverse transcription-PCR (qRT-PCR). Wild-type Bt63 grown on glucose and galactose at 30°C showed no significant changes in expression, while strains grown at 37°C showed an ~4-fold increase in *TGR1* expression on glucose (Fig. 4A).

To next investigate if Tgr1 modulates transcription of genes involved in trehalose metabolism or cellular stress responses, we analyzed transcript levels of both the wild type and mutant at the growth-inhibiting temperature of 37°C on two carbon sources. In addition to six trehalose metabolism genes (*TPS1*, *TPS2*, *NTH1*, and *NTH2*; a putative trehalose synthase gene, *CCG9*; and a putative phosphotrehalase gene, *PTH1*), we examined hexokinase I gene *HXX1* and hexokinase II gene *HXX2*, and components of the calcineurin/calmodulin pathway, the PKC1-MAPK pathway and the cAMP pathway. Trehalose biosynthetic genes have previously been shown in *C. gattii* to regulate components of the cell wall integrity MAPK pathway (32), and yeast trehalose biosynthesis mutants acquire glucose-sensitive (*tps1Δ* and *tps2Δ*) and thermosensitive (*tps2Δ*) phenotypes.

Few significant differences in expression were found for genes involved in trehalose metabolism, and those were primarily related to induction or repression based on the carbon source present (Fig. 4B). However, *HXX1* expression was approximately double wild-type levels in the *tgr1Δ* mutant at 37°C on both glucose and galactose and thus appears to be a general response of *Cryptococcus* to loss of the Tgr1 protein. Hexokinase I was also 3-fold upregulated on galactose in both strains. Expression of stress response genes from a variety of pathways revealed six genes that became unresponsive to galactose-based upregulation in the *tgr1Δ* strain (Fig. 4C). The protein kinase C gene *PKC1*, the calcineurin A gene *CNA1*, the MAPK gene *HOG1*, the Ras protein gene *RAS1*, the adenylyl cyclase gene *CAC1*, and the protein kinase R gene *PKR1* were all upregulated 1.5- to 3-fold on galactose compared to glucose in the wild-type strain; this expression change is abolished in the *tgr1Δ* mutant.

Deletion of *HXX2* ablates the *tgr1Δ* mutant phenotype. Hexokinase is the entry point for nongalactose hexose sugars into glycolysis and is tightly regulated. To determine if altered growth on glucose in the *tgr1Δ* mutant is effected through hexokinase, we examined H99 hexokinase I and hexokinase II mutant strains, H99 (*tgr1Δ-309 hxx1Δ*) and H99 (*tgr1Δ-309 hxx2Δ*), which, by

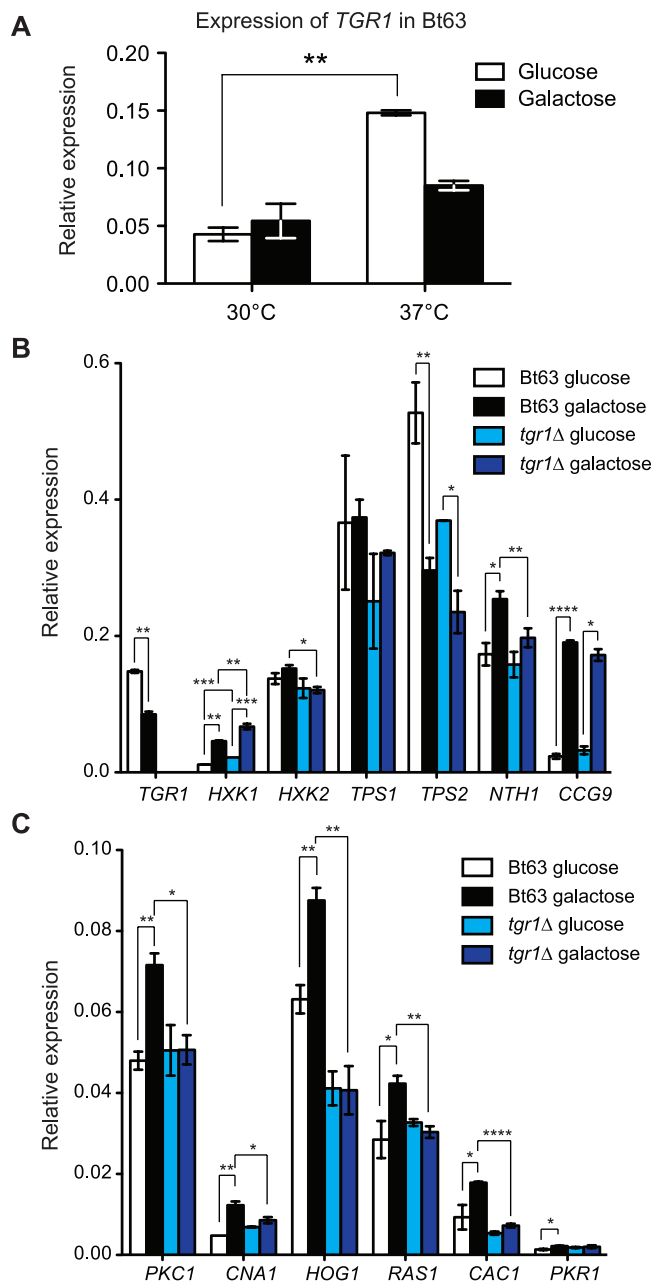


FIG 4 Expression profiling of *TGR1* and genes involved in high-temperature growth and stress responses. Indicated strains were grown on YNB plus glucose or galactose plates for 2 days. (A) Gene expression analysis of *TGR1* in Bt63 at 30°C or 37°C. (B) Expression analysis of trehalose biosynthesis genes and the two hexokinases at 37°C. (C) Gene expression quantification of selected genes implicated in high-temperature growth or cellular stress responses at 37°C. Bars represent means \pm standard errors of gene expression relative to that of β -actin (*ACT1*) from three biological replicates and three technical replicates. *, $P < 0.05$; **, $P < 0.01$; ***, $P < 0.001$; ****, $P < 0.0001$ (Student's two-tailed t test, two sample, equal variance).

virtue of being constructed in H99, also lack *TGR1*. At 37°C, H99 *hxk1*Δ displays normal growth on glucose but reduced growth on galactose, fructose, and mannose, similar to the phenotype of the *C. gattii* R265 *hxk1*Δ strain, which shows reduced growth on galactose (see Fig. S5 in the supplemental material; also results not shown) (32). In contrast, the H99 *hxk2*Δ mutant shows reduced

growth on glucose but not galactose, while the R265 *hxk2*Δ strain displays normal growth on both sugars. Reintroduction of *TGR1* into H99 increases the sensitivity of the strain to high temperature on glucose, confirming the phenotype observed in Bt63. Subsequent reintroduction of *TGR1* into the H99 *hxk2*Δ mutant does not further increase the sensitivity of the strain, however. Deletion of hexokinase II therefore suppresses the phenotype of the *tgr1*Δ mutant in the H99 background.

Metabolite profiling using 1D ^1H NMR reveals increased trehalose levels in the *tgr1*Δ mutant. The Bt63 *tgr1*Δ mutant strain displays more robust growth on glucose at 37°C than does the wild type, suggesting a profound change in intracellular metabolism. To investigate how deletion of *TGR1* affects the metabolome of *Cryptococcus*, we performed one-dimensional (1D) proton nuclear magnetic resonance (NMR) spectroscopy on metabolites extracted from strains Bt63 and Bt63 *tgr1*Δ grown at 37°C on glucose-containing medium. Correlation of spectral peaks with existing metabolite databases and chemical shift standards revealed that the spectra were dominated primarily by signals from sugars, in particular, glucose and trehalose, as well as other metabolites such as succinate, acetate, and glycerol (Fig. 5). To identify sources of variation between the two strains, we performed a multivariate analysis employing principal component analysis (PCA). There was clear separation between the wild-type Bt63 and mutant Bt63 *tgr1*Δ strains in the scores plot of principal components 1 and 2 (Fig. 5); separation along principal component 2 appeared to contain most of the biological variation between the two groups. In the corresponding bivariate loadings plot, which correlates specific metabolites with either the wild type or the mutant, variation in the mutant strain was significantly associated with higher levels of trehalose, fatty acids, and glycerophosphocholine and lower levels of glucose and glycerol than those of the wild type (Fig. 5). Deletion of *TGR1* leading to increased trehalose levels is consistent with our phenotypic observations, as trehalose is accumulated in fungi exposed to a variety of stresses, particularly heat (32).

Bt63 *tgr1*Δ and *yhp2*Δ mutants are unaffected for virulence in the nematode and murine models of cryptococcosis. Strain H99 is the type strain of *C. neoformans* var. *grubii* and was distributed to the community to ensure consistency and veracity of research into the organism's biology and pathogenicity and is the strain used most widely around the world for virulence assays. Utilization of a strain altered for processes such as high-temperature growth and melanization as a standard for virulence models could have ramifications across the *Cryptococcus* research field. To assess the impact on virulence of disruption of these *TGR1* and *YHP2* genes in strain H99, we first investigated the deletion strains in the nematode infection model. There were no significant changes in survival times for *Caenorhabditis elegans* cultured on the Bt63 *tgr1*Δ, *yhp2*Δ, or *tgr1*Δ *yhp2*Δ mutants from the wild-type or complemented strains (Fig. 6). As Yhp2 influences melanization, we repeated the assay in the presence of the melanizable substrate 1-3,4-dihydroxyphenylalanine (L-DOPA); however, no change in virulence was apparent for the Bt63 *yhp2*Δ strain (results not shown). Neither Tgr1 nor Yhp2 appears critical for virulence in the nematode model of cryptococcosis.

As the observed mutant phenotypes occur at 37°C, pathogenicity of both mutants in a mammalian system was determined using the murine inhalation model. Surprisingly, neither the single nor double mutants were significantly altered for virulence, despite

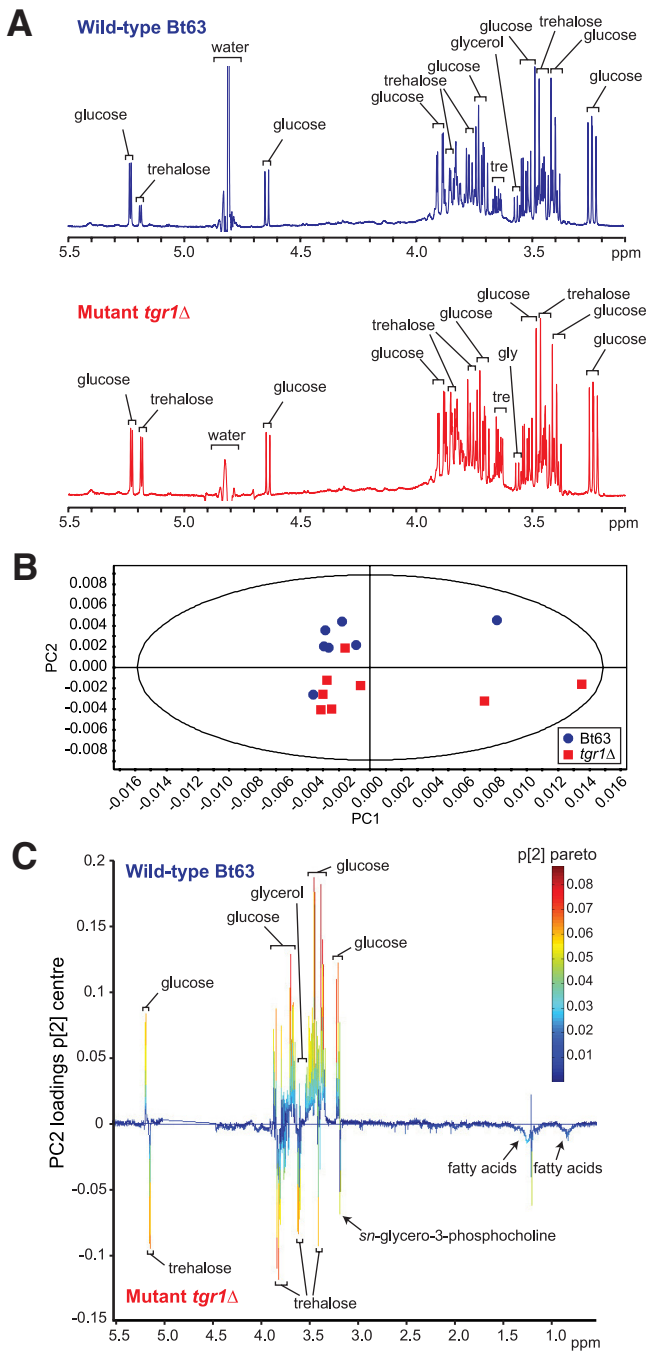


FIG 5 Metabolomics analysis of Bt63 and the *tgr1* Δ mutant strain. (A) 1D proton NMR spectra of wild-type (top, blue) and *tgr1* Δ mutant (bottom, red) strains. Spectra of representative samples for each strain are shown. (B) Principal component analysis scores plot for the wild-type and *tgr1* Δ mutant strains. The distance between the points is an indicator of similarity between the samples. (C) Bivariate loadings line plot. The line plot displays on the loadings coefficient axis the correlation coefficients that relate individual integral regions of the NMR spectrum to the PC2 axis of the scores plot. Individual peaks correspond to peaks in the 1D NMR spectra; here, peaks that are positive indicate metabolites that are increased in the wild-type Bt63 while negative peaks are increased in the *tgr1* Δ mutant. The overlaid heat map relates the correlation of the peak to the PC2 axis of the scores plot when using Pareto scaling instead of center scaling.

TGR1 and *YHP2* affecting multiple cryptococcal virulence factors *in vitro* (Fig. 6). The mutants also displayed wild-type patterns of dissemination, with comparable burdens found in the lungs, brain, liver, spleen, and kidneys (see Fig. S6 in the supplemental material). If there are changes to virulence from these mutants, they are not detectable in this genetic background, although differences may be apparent under certain conditions, such as within an immunocompromised host or by using a lower initial inoculum. Future molecular and pathogenesis studies utilizing H99 will carry an implicit caveat that the strain is atypical for virulence traits and carbon metabolism.

DISCUSSION

Chromosomal rearrangements can contribute to reproductive isolation between closely related fungi and the generation of phenotypic diversity. Variations in karyotype are observed in both clinical and environmental isolates of pathogenic fungi and frequently arise during the infection process (33, 34). Genomic microevolution in *Cryptococcus* and *Candida* may potentially represent an adaptive mechanism within the host environment (22), and changes in karyotype are associated with drug resistance, altered virulence components, and pathogenicity in animal models (35). Such changes are generally tolerated since pathogenic fungi can reproduce mitotically and sexual reproduction and meiosis may be infrequent (36).

Elegant studies utilizing comparative genomics and parsimony analysis have detailed the structural evolution of the genome among the yeasts of the Saccharomycotina. The *Saccharomyces sensu stricto* complex yeasts *Saccharomyces paradoxus*, *Saccharomyces mikatae*, and *Saccharomyces bayanus* are separated from *S. cerevisiae* by ~5 to 20 million years, similar to the *C. neoformans* var. *grubii* and *C. neoformans* var. *neoformans* estimated divergence time of ~24.5 million years (15), and are a useful comparison. Relative to the *S. cerevisiae* genome, *S. paradoxus* possesses four inversions and three duplications, *S. mikatae* possesses four translocations and 13 inversions, and *S. bayanus* possesses five translocations and three inversions (12). The 20 inversions (1 to 30 kb in size) were all flanked by tRNA genes, while one of the duplications (4 to 18 kb in size) and all the translocations were associated with the presence of transposable elements. Our analysis revealed that *C. neoformans* var. *grubii* possesses six inversions (~7 to 81 kb in size) and one duplication (~6 kb in size) that are unique. These were of a similar size as those observed in the *Saccharomyces sensu stricto* complex yeasts, and all but one were associated with a repeated element at the breakpoints, suggesting that the rearrangements are associated with transposon movement and insertion in the genome.

Recently, D'Souza et al. (16) used synteny analysis to compare the genome of *C. gattii* VGI strain WM276 with both the *C. gattii* VGII strain R265 and *C. neoformans* var. *neoformans* VNIV strain B3501A genomes. While the *C. gattii* genomes were broadly colinear, there were widespread rearrangements between the two *C. gattii* genomes and the *C. neoformans* var. *neoformans* genome, including multiple large inversions and translocations associated with transposable elements. The presence of extensive chromosomal rearrangements that differentiate *C. gattii* from *C. neoformans* var. *neoformans* would be expected to significantly impair recombination and chromosome pairing at meiosis and is consistent with a contribution towards speciation (16). Our investigation revealed that only a small number of rearrangements

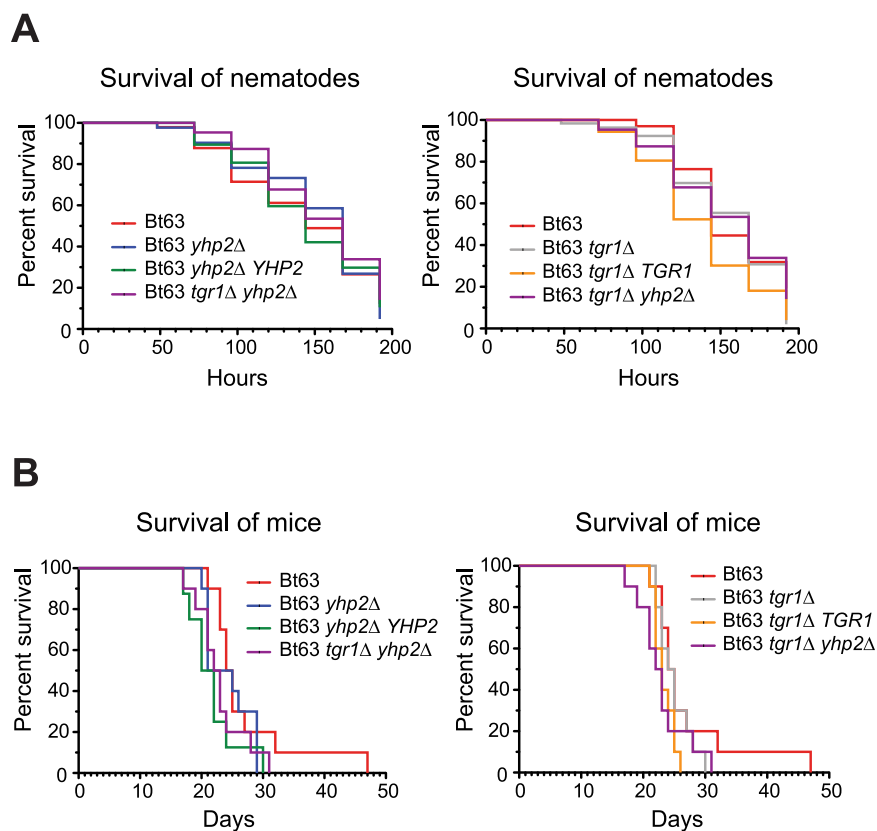


FIG 6 Virulence of translocation gene mutants in the nematode and murine inhalation models of cryptococcosis. (A) Survival times of N2 Bristol nematodes cultured on Bt63, *tgr1*Δ, *tgr1*Δ *TGR1*, *yhp2*Δ, *yhp2*Δ *YHP2*, and *tgr1*Δ *yhp2*Δ strains. (B) Virulence of translocation mutant strains tested *in vivo* using a mouse model system. No nematodes or mice infected with mutant strains were significantly different from those infected with wild-type Bt63.

uniquely distinguish *C. neoformans* var. *grubii* from *C. neoformans* var. *neoformans*, and the profound differences in virulence characteristics and epidemiology may instead be conferred at the nucleotide level. Accordingly, the overall nucleotide sequence divergence level between *C. neoformans* var. *neoformans* and *C. neoformans* var. *grubii*, between 10 and 15%, is substantial and suggests potential speciation (17).

The widely distributed *C. neoformans* var. *grubii* type strain H99 forms the foundation for molecular and pathogenesis studies in *C. neoformans* var. *grubii*. Unfortunately, it is not possible to determine when the translocation occurred, though the absence of additional mutations in both disrupted genes suggests that it was very recent. While it is tempting to suggest that a chromosomal rearrangement that enhanced growth at host body temperature and increased production of two key virulence components may have arisen during infection, *in vivo* virulence studies using nematodes and mice suggest that the gene disruptions did not increase pathogenicity, though they may confer an advantage under specific host conditions or in a different strain background. If the translocation occurred during laboratory passage, it was prior to the distribution of the strain to the wider community as key subcultures all contain it.

The only phenotypes that we could ascribe to the *YHP2* gene product were slight repression of melanization and capsule production. We were excited at the prospect of a potential regulator of

melanin production, a key virulence component of *Cryptococcus*. However, no changes in expression of melanization-related genes were observed in the Bt63 *yhp2*Δ mutant, and since the perturbation of melanin production is very modest, this may be a pleiotropic effect or Yhp2 may instead regulate proteins that potentiate melanin production through other mechanisms, such as uptake of diphenolic precursors or cell wall deposition. Despite the fact that certain subcultures of H99 mate poorly and that homeodomain proteins often regulate developmental processes or sexual reproduction (37), neither *YHP2* nor *TGR1* appears relevant to mating, as we did not observe any changes to hyphal growth or proliferation in unilateral and bilateral crosses using one or both disrupted genes. Future transcriptomic analysis of Bt63 and Bt63 *yhp2*Δ may identify the regulatory targets of the Yhp2 protein.

Trehalose is protective against heat stress and various other cellular stresses in fungi including cell wall stress. Trehalose biosynthesis mutants grow more poorly on glucose at elevated temperatures due to dysregulation of glycolysis and flux through hexokinase II (38); while osmotic stabilizers rescue the phenotype, temperature sensitivity is not restricted to glucose but is common to other hexose sugars and some disaccharides. Our *tgr1*Δ phenotype, however, is restricted solely to

glucose and is not observed on any other hexose or disaccharide, implying that glucose may produce this effect extracellularly. Metabolomics analysis revealed that, primarily, trehalose levels increased and glucose levels decreased in the mutant strain, consistent with our observed phenotype. The cAMP-protein kinase A (PKA) pathway in *Saccharomyces* responds to extracellular glucose stimulus, and intriguingly, a low level of cAMP or reduced PKA pathway activity causes increased heat and stress resistance and accumulation of trehalose (39). As the phenotype is similar, Tgr1 in *Cryptococcus* may potentially modulate cAMP levels directly or indirectly in response to an extracellular glucose signal.

Disruption of *TGR1* and *YHP2* as a result of the H99 translocation will require some caution to be adopted when interpreting genetic, biochemical, and virulence data for the *C. neoformans* var. *grubii* genome strain, particularly in regards to carbon metabolism and signal transduction. As a corollary, the well-characterized *S. cerevisiae* strain S288c possesses a nonsense mutation in *FLO8*, encoding a transcription factor responsible for activation of *FLO11* (40). Lack of Flo11 prevents flocculation and pseudohyphal growth in diploids and invasive growth in haploids in S288c, which is not useful for such studies but remains a good model for other processes. While virulence was unaffected in *C. neoformans* var. *grubii* in two model systems, highlighting that many components beyond traditional virulence factors contribute to successful infection of a host, undoubtedly there remain undiscovered epistatic interactions for both genes that potentially im-

pact pathogenesis. Crucially, each single-gene-deletion strain created using H99, including the *C. neoformans* var. *grubii* gene deletion collection, is effectively a triple deletion strain. Strain H99 has a well-established virulence profile, however, and will remain an important model system for cryptococcal pathogenesis. Carbon metabolism has not been extensively characterized in *C. neoformans* var. *grubii* to date, and this perhaps should be conducted in a separate genetic background from H99. Signaling pathways, however, have been intensively investigated in *Cryptococcus*, and identification of a definitive role for Tgr1 in signal transduction may require some reevaluation or reinterpretation of established interactions and cellular responses.

MATERIALS AND METHODS

Strains and media. *Cryptococcus* strains utilized in this study are listed in Table S1 in the supplemental material. Strains representing VNI AFLP clades were selected from the work of Litvintseva et al. (41). For the translocation PCRs, six H99 subcultures were assayed: from the Heitman lab, H99 #1 (the closest subculture to the original Perfect lab isolate), H99 Wimp, H99 Stud, and H99 #4413. A mixed H99 stock including H99 #1 was passaged through a rabbit and became Stud, and H99 #4413 was a subculture of Stud. From the Lodge lab, we assayed H99 Eunuch, and from the Madhani lab, we assayed H99 CM018, which was derived from Eunuch and is the strain in which the *Cryptococcus* gene deletion collection is being constructed. Wimp and Eunuch were derived from H99 #1 and display attenuated virulence. H99 #1 melanizes poorly while Wimp, Eunuch, and CM018 do not melanize at 37°C. Eunuch and CM018 are sterile while Stud has increased mating proficiency. We also assayed the congenic mating pair KN99 α and KN99 α , which were derived from H99 #4413; the VNI *MATa* isolate 125.91; and the VNII *MATa* isolate 8-1 (42). Cloning applications were performed in the *Escherichia coli* strain MACH1 (Life Technologies, Carlsbad, CA). All chemicals were obtained from Sigma (St. Louis, MO), except nourseothricin (clonNAT), which was from Werner BioAgents (Jena, Germany).

Bioinformatics. The unpublished *C. neoformans* var. *grubii* strain H99 genome is available at the Broad Institute (http://www.broadinstitute.org/annotation/genome/cryptococcus_neoformans/MultiHome.html). Sequence manipulation and dot plot analysis were performed using MacVector 11.0 (MacVector, Cary, NC). Synonymous and nonsynonymous substitution rates were determined using PAL2NAL (43). Sequences for *TGR1* and *YHP2* from Bt63 are available from GenBank under nucleotide accession numbers JQ302192 and JQ302193, respectively.

Molecular techniques. Details of routine molecular techniques are given in Text S1 in the supplemental material. Oligonucleotides utilized in this study are presented in Table S2. *TGR1* and *YHP2* were amplified from Bt63, cloned into pCR2.1-TOPO (Life Technologies), and subcloned into pJAF1 (44) and pPZP-NAT (45), respectively. The *TGR1/YHP2* fusion gene was amplified from H99, cloned into pCR2.1-TOPO, and subcloned into pJAF1.

Phenotypic and virulence factor assays. Extensive details of phenotypic assays and virulence factor assays are given in Text S1 in the supplemental material.

Nematode and murine virulence assays. Virulence of the deletion strains was examined using the *Cryptococcus* nematode model as described elsewhere (46) using *Caenorhabditis elegans* strain N2 Bristol. Murine infection was performed according to the protocol of Cox et al. (47) using 7-week-old BALB/c mice (Animal Resources Centre, Canning Vale, Australia). Ten mice per strain were infected via nasal inhalation with 1×10^5 *Cryptococcus* cells. Mice were monitored for signs of distress or sickness and sacrificed using CO₂ once their body weight had decreased by 20%. Organs were harvested from three mice per strain (the second, fifth, and ninth mice to die), homogenized, and plated to determine fungal CFU per gram organ weight. Kaplan-Meier survival analysis was performed using GraphPad Prism 5.0 (GraphPad Software, La Jolla, CA). Statistical significance was determined using a log-rank test, with a *P* value

of <0.05 being considered significant. Murine virulence assays were conducted in accordance with the guidelines in the Australian code of practice for the care and use of animals for scientific purposes from the National Health and Medical Research Council and were approved by the University of Queensland Molecular Biosciences Ethics Committee (AEC# SCMB/008/11/UQ/NHMRC).

Quantitative real-time PCR. Gene expression analysis via qRT-PCR was performed as described elsewhere (48). Strains were grown on yeast nitrogen base (YNB) plus 2% glucose and YNB plus 2% galactose plates at 37°C or in liquid melanization medium (with or without L-DOPA) at 30°C and were harvested after 24 h. cDNA was synthesized using Superscript III (Life Technologies). Real-time PCR primers are found in Table S2 in the supplemental material. Relative gene expression was evaluated using the threshold cycle ($2^{-\Delta\Delta CT}$) method normalized against β -actin. Statistical significance was determined using an unpaired Student's *t* test in GraphPad Prism, where $P < 0.05$ was considered significant.

1D ¹H NMR spectroscopy. Bt63 and Bt63 *tgr1* Δ strains were cultured on YNB plus 2% glucose at 37°C, harvested after 48 h, and lyophilized. Metabolite extraction was performed using the yeast extraction protocol of Lewis et al. (49). For ¹H NMR analysis, extracts were resuspended in 100 mM potassium phosphate buffer (pH 7.4), 10% D₂O, 18 μ M 2,2-dimethylsilapentane-5-sulfonic acid (DSS), and 18 μ M 1,1-difluoro-1-trimethylsilylphosphonic acid in 5-mm NMR tubes. NMR spectroscopy was performed on a Bruker AV500 500-MHz spectrometer (Bruker Biospin, Rheinstetten, Germany), equipped with a 5-mm self-shielded z-gradient triple resonance probe. Spectra were measured manually at 298 K with 200 scans at 32k resolution with a spectral width of 14 ppm, using the noesy1prd pulse program (Bruker pulse program library). Low-power continuous wave irradiation was applied during the mixing time of 100 ms and relaxation delay of 2.3 s to suppress the water signal.

Metabolite profiling. 1D spectra were processed using Topspin 3.0 (Bruker Biospin). Spectra were reduced to 0.001-ppm integral regions using AMIX 3.6.6 (Bruker Biospin); regions corresponding to the water signal were excluded ($\delta = 4.5$ ppm to 5.05 ppm), and data were normalized to the total intensity of the spectrum. Principal component analysis (PCA) with center scaling was performed in SIMCA-P⁺ 12.0 (Umetrics AB, Sweden). The refined model comprised 15 samples and contained 2 principal components, with an *R*²X value of 0.83 and a *Q*² value (from cross-validation) of 0.684. To gauge the contributions from weaker NMR signals more accurately, the 1D loading plot of principal component 2 of the center-scaled model was heat mapped with the corresponding loadings coefficients from a Pareto-scaled PCA model (5 principal components; *R*²X = 0.837, *Q*² = 0.47). Metabolites were identified using ChemX NMR suite 7.1 (ChemX, Edmonton, Canada) and the public databases BioMagRes Data Bank (<http://www.bmrw.wisc.edu>) and Human Metabolome Data Bank (<http://www.hmdb.ca>).

ACKNOWLEDGMENTS

This work was supported by NHMRC project grant no. 455980 and NHMRC CDA 569673 to J.A.F. C.A.M. was supported by an ANZ Trustees PhD Scholarship in Medical Research. E.J.B. and J.H. were supported by NIH/NIAID grant R37 AI39115 to J.H. K.N. was supported by NIH grant AI080275.

SUPPLEMENTAL MATERIAL

Supplemental material for this article may be found at <http://mbio.asm.org/lookup/suppl/doi:10.1128/mBio.00310-11/-DCSupplemental>.

Text S1, DOCX file, 0.1 MB.

Figure S1, PDF file, 0.4 MB.

Figure S2, PDF file, 0.2 MB.

Figure S3, PDF file, 1.1 MB.

Figure S4, PDF file, 0.8 MB.

Figure S5, PDF file, 0.3 MB.

Figure S6, PDF file, 0.2 MB.

Table S1, DOCX file, 0.1 MB.

Table S2, DOCX file, 0.1 MB.

REFERENCES

- Stranger BE, et al. 2007. Relative impact of nucleotide and copy number variation on gene expression phenotypes. *Science* 315:848–853.
- Rieseberg LH. 2001. Chromosomal rearrangements and speciation. *Trends Ecol. Evol.* 16:351–358.
- Delneri D, et al. 2003. Engineering evolution to study speciation in yeasts. *Nature* 422:68–72.
- Rieseberg LH, Willis JH. 2007. Plant speciation. *Science* 317:910–914.
- Navarro A, Barton NH. 2003. Accumulating postzygotic isolation genes in paraparty: a new twist on chromosomal speciation. *Evolution* 57:447–459.
- Wain LV, Armour JA, Tobin MD. 2009. Genomic copy number variation, human health, and disease. *Lancet* 374:340–350.
- Sturtevant AH, Dobzhansky T. 1936. Inversions in the third chromosome of wild races of *Drosophila pseudoobscura*, and their use in the study of the history of the species. *Proc. Natl. Acad. Sci. U. S. A.* 22:448–450.
- Charlesworth B. 1991. The evolution of sex chromosomes. *Science* 251:1030–1033.
- Fraser JA, et al. 2004. Convergent evolution of chromosomal sex-determining regions in the animal and fungal kingdoms. *PLoS Biol* 2:2243–2255.
- Harewood L, et al. 2010. The effect of translocation-induced nuclear reorganization on gene expression. *Genome Res.* 20:554–564.
- Taylor JS, Braasch I, Frickey T, Meyer A, Van de Peer Y. 2003. Genome duplication, a trait shared by 22000 species of ray-finned fish. *Genome Res.* 13:382–390.
- Kellis M, Birren BW, Lander ES. 2004. Proof and evolutionary analysis of ancient genome duplication in the yeast *Saccharomyces cerevisiae*. *Nature* 428:617–624.
- Park BJ, et al. 2009. Estimation of the current global burden of cryptococcal meningitis among persons living with HIV/AIDS. *AIDS*. 23:525–530.
- Heitman J, Kozel TR, Kwon-Chung KJ, Perfect JR, Casadevall A (ed). 2010. *Cryptococcus*: from human pathogen to model yeast. ASM Press, Washington, DC.
- Ngamskulrungraj P, et al. 2009. Genetic diversity of the *Cryptococcus* species complex suggests that *Cryptococcus gattii* deserves to have varieties. *PLoS One* 4:e5862.
- D'Souza CA, et al. 2011. Genome variation in *Cryptococcus gattii*, an emerging pathogen of immunocompetent hosts. *mBio* 2:e00342–10.
- Kavanaugh LA, Fraser JA, Dietrich FS. 2006. Recent evolution of the human pathogen *Cryptococcus neoformans* by intervarietal transfer of a 14-gene fragment. *Mol. Biol. Evol.* 23:1879–1890.
- Sun S, Xu J. 2009. Chromosomal rearrangements between serotype A and D strains in *Cryptococcus neoformans*. *PLoS One* 4:e5524.
- Fries BC, Chen F, Currie BP, Casadevall A. 1996. Karyotype instability in *Cryptococcus neoformans* infection. *J. Clin. Microbiol* 34:1531–1534.
- Spitzer ED, Spitzer SG, Freundlich LF, Casadevall A. 1993. Persistence of initial infection in recurrent *Cryptococcus neoformans* meningitis. *Lancet* 341:595–596.
- Selmecki A, Forche A, Berman J. 2006. Aneuploidy and isochromosome formation in drug-resistant *Candida albicans*. *Science* 313:367–370.
- Forche A, Magee PT, Selmecki A, Berman J, May G. 2009. Evolution in *Candida albicans* populations during a single passage through a mouse host. *Genetics* 182:799–811.
- Perfect JR, Casadevall A. 2010. The history of *Cryptococcus* and cryptococcosis, p. 17–26. In Heitman J, Kozel TR, Kwon-Chung KJ, Perfect JR, Casadevall A (ed), *Cryptococcus*: from human pathogen to model yeast. ASM Press, Washington, DC.
- Fraser JA, et al. 2005. Chromosomal translocation and segmental duplication in *Cryptococcus neoformans*. *Eukaryot. Cell* 4:401–406.
- Kirkpatrick M, Barton N. 2006. Chromosome inversions, local adaptation and speciation. *Genetics* 173:419–434.
- Simsek D, Jasin M. 2010. Alternative end-joining is suppressed by the canonical NHEJ component Xrcc4-ligase IV during chromosomal translocation formation. *Nat. Struct. Mol. Biol* 17:410–416.
- Kopecká M, Gabriel M. 1992. The influence of Congo red on the cell wall and (1–3)- β -D-glucan microfibril biogenesis in *Saccharomyces cerevisiae*. *Arch. Microbiol* 158:115–126.
- de Souza Pereira R, Geibel J. 1999. Direct observation of oxidative stress on the cell wall of *Saccharomyces cerevisiae* strains with atomic force microscopy. *Mol. Cell. Biochem.* 201:17–24.
- Alspaugh JA, et al. 2002. Adenylyl cyclase functions downstream of the $G\alpha$ protein Gpa1 and controls mating and pathogenicity of *Cryptococcus neoformans*. *Eukaryot. Cell* 1:75–84.
- Idnurm A, Giles SS, Perfect JR, Heitman J. 2007. Peroxisome function regulates growth on glucose in the basidiomycete fungus *Cryptococcus neoformans*. *Eukaryot. Cell* 6:60–72.
- Petzold EW, et al. 2006. Characterization and regulation of the trehalose synthesis pathway and its importance in the pathogenicity of *Cryptococcus neoformans*. *Infect. Immun.* 74:5877–5887.
- Ngamskulrungraj P, et al. 2009. The trehalose synthesis pathway is an integral part of the virulence composite for *Cryptococcus gattii*. *Infect. Immun.* 77:4584–4596.
- Selmecki A, Gerami-Nejad M, Paulson C, Forche A, Berman J. 2008. An isochromosome confers drug resistance *in vivo* by amplification of two genes, *ERG11* and *TAC1*. *Mol. Microbiol* 68:624–641.
- Hu G, et al. 2008. Comparative hybridization reveals extensive genome variation in the AIDS-associated pathogen *Cryptococcus neoformans*. *Genome Biol* 9:R41.
- Fries BC, Casadevall A. 1998. Serial isolates of *Cryptococcus neoformans* from patients with AIDS differ in virulence for mice. *J. Infect. Dis.* 178:1761–1766.
- Morrow CA, Fraser JA. 2009. Sexual reproduction and dimorphism in the pathogenic basidiomycetes. *FEMS Yeast Res.* 9:161–177.
- Hull CM, Boily MJ, Heitman J. 2005. Sex-specific homeodomain proteins Sxl α and Sxl2 α coordinately regulate sexual development in *Cryptococcus neoformans*. *Eukaryot. Cell* 4:526–535.
- Hohmann S, Bell W, Neves MJ, Valckx D, Thevelein JM. 1996. Evidence for trehalose-6-phosphate-dependent and -independent mechanisms in the control of sugar influx into yeast glycolysis. *Mol. Microbiol* 20:981–991.
- Verselle M, de Winde JH, Thevelein JM. 1999. A novel regulator of G protein signalling in yeast, RGS2, downregulates glucose-activation of the cAMP pathway through direct inhibition of Gpa2. *EMBO J.* 18:5577–5591.
- Liu H, Styles CA, Fink GR. 1996. *Saccharomyces cerevisiae* S288C has a mutation in *FLO8*, a gene required for filamentous growth. *Genetics* 144:967–978.
- Litvintseva AP, Thakur R, Vilgalys R, Mitchell TG. 2006. Multilocus sequence typing reveals three genetic subpopulations of *Cryptococcus neoformans* var. *grubii* (serotype A), including a unique population in Botswana. *Genetics* 172:2223–2238.
- Nielsen K, et al. 2003. Sexual cycle of *Cryptococcus neoformans* var. *grubii* and virulence of congenic α and β isolates. *Infect. Immun.* 71:4831–4841.
- Suyama M, Torrents D, Bork P. 2006. PAL2NAL: robust conversion of protein sequence alignments into the corresponding codon alignments. *Nucleic Acids Res.* 34:W609–W612.
- Fraser JA, Subaran RL, Nichols CB, Heitman J. 2003. Recapitulation of the sexual cycle of the primary fungal pathogen *Cryptococcus neoformans* var. *gattii*: implications for an outbreak on Vancouver Island, Canada. *Eukaryot. Cell* 2:1036–1045.
- Idnurm A, Reedy JL, Nussbaum JC, Heitman J. 2004. *Cryptococcus neoformans* virulence gene discovery through insertional mutagenesis. *Eukaryot. Cell* 3:420–429.
- Mylonakis E, Ausubel FM, Perfect JR, Heitman J, Calderwood SB. 2002. Killing of *Caenorhabditis elegans* by *Cryptococcus neoformans* as a model of yeast pathogenesis. *Proc. Natl. Acad. Sci. U. S. A.* 99:15675–15680.
- Cox GM, Mukherjee J, Cole GT, Casadevall A, Perfect JR. 2000. Urease as a virulence factor in experimental cryptococcosis. *Infect. Immun.* 68:443–448.
- Lee IR, Chow EW, Morrow CA, Djordjevic JT, Fraser JA. 2011. Nitrogen metabolite repression of metabolism and virulence in the human fungal pathogen *Cryptococcus neoformans*. *Genetics* 188:309–323.
- Lewis IA, et al. 2007. Method for determining molar concentrations of metabolites in complex solutions from two-dimensional ^1H - ^{13}C NMR spectra. *Anal. Chem.* 79:9385–9390.